Forsman, Nina; Österberg, Monika; Johansson, Leena-Sisko; Kääriäinen, Pirjo; Tuure, Matilda; Koivula, Hanna

Open coating with natural wax particles enables scalable, non-toxic hydrophobation of cellulose-based textiles

Published in:
Carbohydrate Polymers

DOI:
10.1016/j.carbpol.2019.115363

Published: 01/01/2020

Document Version
Peer-reviewed accepted author manuscript, also known as Final accepted manuscript or Post-print

An electroactive alginate hydrogel nanocomposite reinforced by functionalized graphite nanofilaments for neural tissue engineering

Shahin Homaeigohar [a,*], Ting-Yu Tsai [b], Tai-Hong Young [b], Hsin Ju Yang [b], You-Ren Ji [b]
a: School of Chemical Engineering, Department of Chemistry and Materials Science, Aalto University, Kemistintie 1, 00076 Aalto, Finland.
b: Institute of Biomedical Engineering, National Taiwan University, No.1, Sec. 1, Jen-Ai Rd., Taipei 100, Taiwan
*Corresponding Author's e-Mail: shahin.homaeigohar@aalto.fi.

Abstract
To address the need to biodegradable, electroactive conduits accelerating nerve regeneration, here we develop a nanocomposite hydrogel made of alginate reinforced by citric acid functionalized graphite nanofilaments. The green, simple functionalization enhances the nanofillers distribution and their biocompatibility, as verified using mesenchymal stem cells *in vitro*. The uniformly distributed nanofilaments raise mechanical stability of the nanocomposite hydrogel versus the neat one up to three times. Also, the nanofilaments enable electrical contact and intercellular signaling thereby stimulating their biological activity. *In vitro* studies proved the biocompatibility of the nanocomposite hydrogel whereon PC12 cells proliferate and spread evidently. *In vivo* tests also supported applicability of the nanocomposite hydrogel for implantation within body, and the samples showed no adverse reaction and no inflammatory responses after 14 days. Conclusively, the results certify that the developed electroactive nanocomposite hydrogel is able to stimulate nerve generation and could be confidently used as a nerve conduit material.
Keywords: nerve, tissue engineering, hydrogel, graphite, electroactivity.

1. Introduction

Peripheral nerve injury (PNI) imposes a large burden to medical society and over 1 million patients across the world deal with this crisis annually (Rebowe et al., 2018). This problem can lead to severe disability in 24-41% of patients suffering from a notable upper extremity PNI after only one year, in case no proper treatment is adopted (Rebowe et al., 2018). In the cases where tensionless nerve repair is impossible, nerve autografting is considered as the benchmark therapy (Griffin, Hogan, Chhabra, & Deal, 2013; Li et al., 2014). However,

there are several related challenges including lack of donor nerve, extended operating time, morbidity of the donor site, and disability (Kehoe, Zhang, & Boyd, 2012). In addition, only the nerve gaps as small as 5 cm or even shorter can be repaired by autografts (Rebowe et al., 2018; Siemionow & Brzezicki, 2009). Considering all these shortcomings, there is a demand for the peripheral nerve repairs by advanced nerve grafting substitutes. In this regard, neural tissue engineering relying on biodegradable polymeric conduits has shown a promising applicability (X. Liu et al., 2016). Different biodegradable polymers including chitosan (Muheremu et al., 2017), collagen (Yao et al., 2018), fibrin (Wang et al., 2018), poly(ethylene glycol) (PEG)(X. Liu et al., 2016), poly-lactic-co-glycolic acid (PLGA)(Yin et al., 2018), poly-L-lactide acid (PLLA)(Frost et al., 2018), polycaprolactone (PCL)(Lopez et al., 2018), and poly(caprolactone fumarate) (PCLF)(Golafshan, Gharibi, Kharaziha, & Fathi, 2017) have been investigated for the sake of nerve regeneration through the conduits made thereof. Alginate is an anionic polysaccharide extracted from seaweed that is composed of mannuronic acid and guluronic acid units. It is formed as a hydrogel when an ionic bonding between the carboxylate group of its backbone and a cationic crosslinking agent such as Ca^{2+}, Zn^{2+}, Ba^{2+}, Al^{3+} takes place (Z. Shi et al., 2016). Alginate can offer enzymatic degradability, optimum biocompatibility, negligible inflammatory response, remarkable chemical flexibility and resemblance to the extracellular matrix structure (Kim & Kim, 2014). Alginate hydrogels have shown promising applicability with respect to various biomedical applications such as tissue engineering scaffold (Marrella et al., 2017; Reakasame & Boccaccini, 2017), drug delivery (Guarino, Altobelli, della Sala, Borzacchiello, & Ambrosio, 2018) among others. Concerning neural tissue engineering, alginate has been extensively employed in construction of nerve conduits (Hashimoto et al., 2005; Prang et al., 2006). Yet, the neural scaffolds based on alginate are mechanically weak thus unable to bear physiological loading conditions and suffer from high degradation rate (Golafshan, Kharaziha, & Fathi, 2017). This drawback justifies blending of alginate with other polymers such as PCL (Kim & Kim, 2014), polyacrylamide (Omidian, Rocca, & Park, 2006), polyvinyl alcohol (PVA)(Shen & Hsieh, 2014) and also its hybridization by incorporating nanofillers. With respect to the latter option, various nanofillers have been suggested for the composite biomaterials (S. S. Homaeigohar, Sadi, Javadpour, & Khavandi, 2006; S. S. Homaeigohar et al., 2005; Sadi et al., 2006; Yari Sadi, Shokrgozar, Homaeigohar, & Khavandi, 2008), but the conductive ones not only enhance mechanical stability and durability of the hydrogel but also confer the material with electrical conductivity. In particular, for neural tissue engineering, and to encourage material-neuron interaction leading to neuron regeneration, conductive nanomaterials including polypyrrole (G. Shi, Rouabhia, Wang, Dao, & Zhang,

2004), silver (Ding et al., 2011), gold (Lin, Jen, Hsu, & Chiu, 2008), carbon nanotubes (Mottaghitalab et al., 2013), and graphene (Golafshan, Kharaziha, et al., 2017) have been examined. It has been reported that this kind of nanohybridization can result in the enhancement of neural cell response *in vitro* and induction of axon growth *in vivo* (Brett Runge et al., 2010; Vivó et al., 2008). Among the carbon nanomaterials family, carbon nanotubes and graphene are indeed the most widely studied ones, particularly for neural tissue engineering scaffolds (J. H. Lee, Lee, Yang, Lee, & Kim, 2014; X. Liu et al., 2016; Mehrali et al., 2017). One big challenge related to such carbon nanomaterials is their large aggregation tendency when suspended within viscous polymeric solutions**.** The resulting aggregation leads to non-uniform distribution of the carbon nanofillers and therefore anisotropic conductivity and mechanical properties within the hydrogel host. Moreover, in case the carbon nanofillers are not chemically functionalized, their presence within hydrogel is solely governed by physical entanglement. Subsequently, subjected to aqueous biological solutions, the hydrogel is expanded and weakens the entanglements of the carbon nanofillers, leading to the likely release of them into the human body. Accordingly, to develop electroactive, robust neural scaffolds, based on alginate hydrogel, there is a need to functional conductive carbon nanofillers with the least agglomeration problem.

In this study, for the first time, we employ citric acid (CA) functionalized graphite nanofilaments (CAGNFs) to improve electrical, mechanical, and biological properties of an alginate hydrogel for neural tissue engineering. CA functionalization is a simple, green approach to induce formation of oxygen containing functional groups on the surface of graphite nanofilaments, thereby assuring their uniform distribution within the alginate matrix. As the main hypothesis of our study, we postulate that inclusion of the CA functionalized graphite nanofilaments into an alginate matrix engenders higher mechanical stability for the resulting hydrogel nanocomposite. Additionally, the conductive graphite nanofilaments provide local conductive zones, thereby enabling intercellular signaling and optimizing neural cells activities. Thanks to electrical conductivity, improved durability and less degradation rate, nerve cells can grow and regenerate on the nanocomposite hydrogel. To the best of our knowledge, carbon nanofibers have been rarely and almost never used in development of an electroactive, mechanically robust scaffold or conduit for nerve regeneration. Thus, our approach is considered a novel method for construction of neural tissue engineering scaffolds that is beyond state of the art.

2. Materials and Methods

2.1. Materials

Alginate (Alginic acid sodium salt from brown algae) and Citric acid (citric acid monohydrate, ACS reagent ≥ 99.0%) were purchased from Sigma Aldrich (Saint Louis, MO, USA). Polyacrylonitrile (PAN) (200,000 $g \cdot mol^{-1}$, purity 99.5%) and dimethylformamide (DMF) (purity 99%) were purchased from Dolan GmbH (Kelheim, Germany) and Merck (Darmstadt, Germany), respectively. Water as the solvent for alginate was deionized water.

2.2. Synthesis and characterization of CAGNFs

The CAGNFs were prepared according to our previously reported approach and based on pyrolysis of PAN precursor nanofibers (S. Homaeigohar & Elbahri, 2019; S. Homaeigohar, Strunskus, Strobel, Kienle, & Elbahri, 2018). First, the PAN nanofibers were made through electrospinning of a PAN solution (8 wt % in DMF) with a feed rate of 1 $mL \cdot h^{-1}$ and under a voltage of 20 kV. The PAN nanofibers were oxidized in air at 250 °C for 2 h and then graphitized under argon atmosphere at 1250 °C for half an hour with a heating rate of 5 $°C \cdot min^{-1}$. Eventually, the graphitized nanofibers were cooled down to room temperature with a cooling rate of 5 $°C \cdot min^{-1}$.

While the graphite nanofibers are produced in a one pot, inexpensive manner via pyrolysis of PAN nanofibers, they can be greenly functionalized by addition of CA (30 $mg \cdot mL^{-1}$) in their aqueous suspension (3 mg in 10 mL water) to be ultrasonicated (2 min at a power of 20%). It is worthy to note that the graphite nanofibers are disintegrated as nanofilaments, that ease the subsequent nanocomposite processing, and are simultaneously functionalized during the ultrasonication stage. The nanofilaments are amphiphilic and composed of a large graphitic fraction along with a minor oxygenated amorphous carbon one. As we previously proved (S. Homaeigohar & Elbahri, 2019), functionalization of the GNFs through the citric acid treatment leads to emergence of oxygen based functional groups including carbonyl and hydroxyl on the surface of the nanofilaments. This feature enables a bilateral interaction between the carboxyl and hydroxyl groups of alginate and CAGNFs, thus leading to improved mechanical stability and filler distribution i.e. isotropicity. The morphology and size of the CAGNFs was determined by scanning electron microscopy (SEM) (LEO 1550VP Gemini from Carl ZEISS, Jena, Germany) and atomic force microscopy (AFM) (MultiMode^{TM} Atomic Force Microscope from Bruker AXS, Madison, WI, USA). The electrical conductivity of the CAGNFs (cast as a freestanding membrane via a vacuum filtration process) was characterized by a four-point probe test. The thickness of the membrane required

for the measurement was already assessed by a digital micrometer (Deltascope® MP2C from Fischer, Windsor, CT, USA).

2.3. Construction of CAGNF-Alginate nanocomposite scaffolds

As schematically demonstrated in Figure 1, the alginate solution was prepared by dissolving 3 gr alginate in 100 ml distilled water. To prepare the nanocomposite hydrogels, 1 mg CAGNFs were suspended into the alginate solution to make nanocomposite hydrogels with the nanofiller concentration of 0.6 wt.%. The resulting suspension was stirred overnight at room temperature to homogenize distribution of the nanofilaments and then $CaCl_2$ (Calcium Chloride, Anhydrous, 0.25 molar; Baker Analyzed, ACS Reagent, Avantor, USA) was added as the cross linker. The cross linking treatment took 40 min at room temperature. Upon completion of the crosslinking process, the samples were soaked in excess deionized water for 48 hours and water was refreshed every 12 hours to eliminate any remaining impurities. Eventually, the hydrogels were cast as films with given dimensions of 10x20x1 (width (W) x length (L) x Height (H)) mm^3 and air dried at room temperature overnight.

2.4. Structural Characterization of the nanocomposite scaffolds

The molecular weight (M_w) of alginate was determined by gel permeation chromatography (GPC 1100 Agilent) and by using THF as the eluent. The mannuronate/guluronate (M/G) ratio of alginate was measured based on the circular dichroism (CD) spectra. A solution of the sodium salt of the sample, at a concentration of 5×10^{-3} monomol/L, was prepared in deionised water, and the pH was adjusted to 7. The CD spectra were obtained by a circular dichroism spectrometer (Jasco J-815) (λ= 195–250 nm) (bandwidth= 1 nm and time per point= 0.5 s). The d-mannuronate/l-guluronate ratio was quantified via the following equations (Florea-Spiroiu, Bala, Balan, Nichita, & Stamatin, 2012):

$$\text{Mannuronate/guluronate} \approx 2(\text{peak/trough}) \text{ if peak/trough} < 1 \quad (1)$$

$$\%\text{Mannuronate} \approx 27(\text{peak/trough}) + 40 \text{ if peak/trough} > 1 \quad (2)$$

Viscosity of the alginate solution with and without the CAGNFs was measured at room temperature by a rotational viscometer (Rapid Visco Analyzer, RVA) at a constant stirring speed of 160 rpm. Surface chemistry of alginate and the nanocomposite made thereof was determined by ATR-FTIR (ALPHA (ATR-Ge, ATR-Di) from BRUKER Optik GmbH, Ettlingen, Germany). Electrical conductivity of the nanocomposite and pure hydrogels was measured from the resistivity of 5 cuboid samples with the aforementioned dimensions. The electrical

resistance (R) of the nanocomposite hydrogel sheets was determined by a Fluke 73 multimeter (Washington, USA). Sheet resistivity (ρ) was quantified using the equation (3):

$$\rho = R\frac{W\times H}{L} \quad (3)$$

The conductivity of the hydrogels (σ) ($S.m^{-1}$) is the reciprocal of resistivity.

The distribution of the CAGNFs within the alginate matrix was characterized by optical microscopy (Olympus LX71, Tokyo, Japan). Mechanical properties of the neat alginate and CAGNF/alginate (1cm x 2cm x 0.1cm) were tested by a uniaxial tensile tester (Bose ElectroForce 5500, TA instruments, Delaware, USA). At least 5 samples of each group of alginate and nanocomposite hydrogel were tested. The swelling percentage of hydrogels (nanocomposite and neat) immersed in phosphate buffer saline (PBS) (pH7.4) that could imply the larger void volume in the nanocomposite hydrogels was determined by recording their weight variations for a 24 hour period at room temperature. The swelling percentage was calculated via the following equation (4):

$$Swelling\ percentage = \frac{(W_t - W_0)}{W_0}\times 100\% \quad (4)$$

where W_t and W_0 represent the weight of the samples at a given interval and at onset of the experiment after immersion in PBS.

To calculate the porosity, 3 cuboid samples with given dimensions thus volume of each category of the neat and nanocomposite hydrogels were weighed using an electronic balance (a resolution of 0.1 mg). The apparent density (ρ) of the samples were determined from the obtained mass and the volume. The porosity (ε) can be then quantified via the following equation (5)(S. Homaeigohar, Dai, & Elbahri, 2013; S.Sh. Homaeigohar, H. Mahdavi, & Elbahri, 2012):

$$\varepsilon = \frac{(\rho_0 - \rho)}{\rho_0}\times 100\% \quad (5)$$

where ρ_0 is the average density of the materials used in fabrication of the samples and can be calculated via the equation (6):

$$\frac{1}{\rho_0} = \frac{\varphi_{alginate}}{\rho_{alginate}} + \frac{\varphi_{GNF}}{\rho_{GNF}} \quad (6)$$

where $\rho_{alginate}$ and ρ_{GNF} are 1.6 and 2.1 g/cm^3 , respectively. $\phi_{alginate}$ and ϕ_{GNF} are mass fractions of the components.

2.5. Biological Characterization of the nanocomposite scaffolds

The biocompatibility and the stimulation ability of the nanocomposite hydrogels for PC12 cell adhesion, proliferation and neuronal differentiation were also extensively monitored.

As schematically illustrated in Figure 1, the nerve cell growth and differentiation on the nanocomposite hydrogels were imaged, as well. The effect of CA functionalization on the biocompatibility of the GNFs was also surveyed using MSCs *in vitro*. Eventually, the nanocomposite hydrogel was implanted in the Guinea pigs' body to further evaluate the biocompatibility *in vivo*.

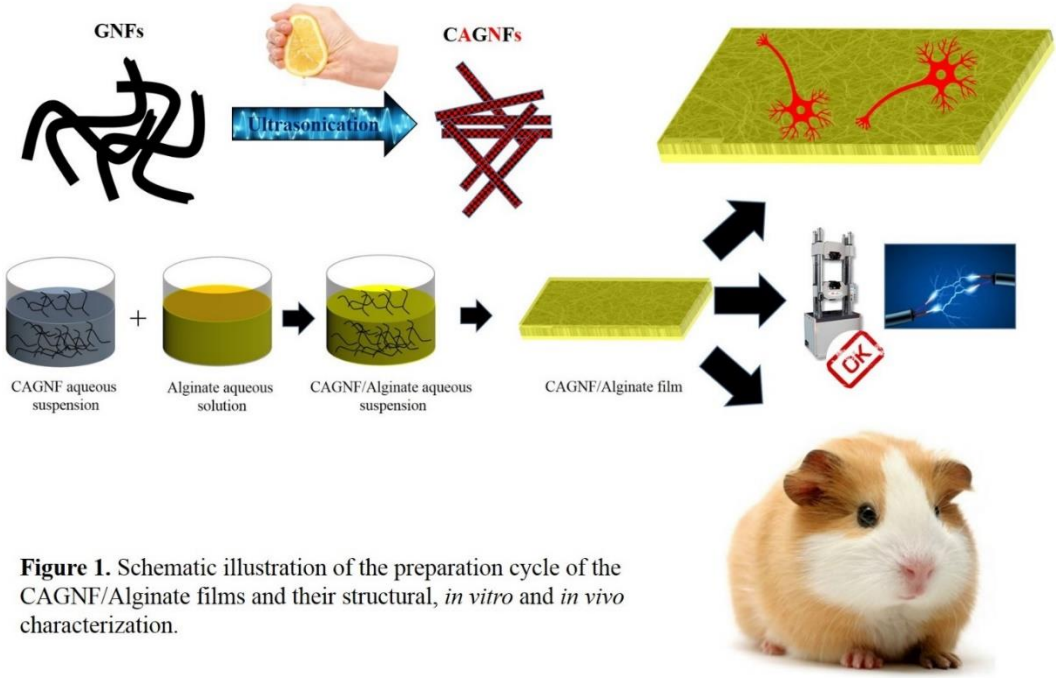

Figure 1. Schematic illustration of the preparation cycle of the CAGNF/Alginate films and their structural, *in vitro* and *in vivo* characterization.

2.5.1. Cytotoxicity and proliferation test

The GNFs as non- and CA functionalized were evaluated in terms of cytotoxicity effect on the MSCs *in vitro*. The cells were cultured in the low glucose Dulbecco's Modified Eagle Medium (DMEM) supplemented with 10% fetal bovine serum, and 1% streptomycin/penicillin, and incubated (under 95% relative humidity, 5% CO_2, and at 37 °C). The MSCs were counted and seeded at a concentration of 3,000 cells.cm^{-2} in 24 wells. After seeding the cells, 50 µl GNF and CAGNF suspension with the concentration of 0.005% was added into each well. During the cell culturing period (5 days), the MTT assay (Roche Applied Science, Mannheim, Germany) was performed at each day to quantify the cell number. The absorbance value was read at 570 nm by an ELISA Reader (SpectraMax Plus 384, Molecular Devices, Sunnyvale, CA).

The cross linked hydrogels with the dimensions of 2cm x 2cm x 0.1 cm (LxWxH) were immersed in deionized water for 48 hours (refreshed thrice) to wash off the uncross linked polymer as well as the remaining cross linkers. Afterwards, the hydrogels were sterilized by UV irradiation for one hour and then washed with the sterilized PBS at least five times in three days. The sterilized samples were fixed in the bottom of the wells (of a 12 well tissue culture

plate) and presaturated with Roswell Park Memorial Institute (RPMI) supplemented with 10% horse serum, 5% fetal bovine serum, and 0.5% streptomycin/penicillin for two hours before cell seeding. The PC12 cells were cultured in the RPMI medium supplemented with 5% fetal bovine serum, 10% horse serum, and 0.5% streptomycin/penicillin. The cell suspension was placed in the cell culture incubator (95% relative humidity, 5% CO_2 and 37 ºC). After trypsinization, the PC12 cells were re-suspended in RPMI, counted, and seeded at a concentration of 30,000 cells.cm^{-2} in the 12-well tissue culture polystyrene (TCPS) plates whose several wells were partly occupied by the nanocomposite hydrogel samples. After 1,4, and 7 days of incubation in the RPMI supplemented with 10% horse serum, 5% fetal bovine serum, and 0.5% streptomycin/penicillin, the cell number was quantified through the WST-1 assay (Roche Applied Science, Mannheim, Germany). The absorbance value was read at 436 nm by a UV−visible absorbance microplate reader (SpectraMax Plus 384, Molecular Devices, Sunnyvale, CA).

2.5.2. Neuronal differentiation test

The morphological characteristics of neurons, particularly in terms of neurite outgrowth, were determined by optical microscopy and also via staining of PC12 cells. The PC12 cells were seeded on the two types of hydrogels at a density of 22,000 cells. cm^{-2} and cultured in the RPMI supplemented with 10% horse serum, 5% fetal bovine serum, and 0.5% streptomycin/penicillin for 12 h to allow attachment. The cells on hydrogels were then induced by adding 50 ng.ml^{-1} nerve growth factor (NGF) into the medium and incubation for 4 days. The differentiated PC12 cells were fixed with a 4% paraformaldehyde (PFA) solution and permeabilized by a 1% Triton X-100 solution. Immunostaining of the cells was conducted sequentially with rhodamine−phalloidin (RP, red) and DAPI to visualize the F-actin arrangement and cell nuclei, respectively. The fluorescent images of the stained cells were taken by a fluorescence microscope (Leica DFC360 FX). The captured fluorescent images were subsequently analyzed in terms of the cell expanding area, number i.e. percentage of the cells with neurites, and average neurite length using the ImageJ software.

2.5.3. *In vivo* test

The *in vivo* biocompatibility and degradation of the nanocomposite hydrogel were evaluated by implanting them in the subcutaneous tissues of three two-year-old guinea pigs. Each guinea pig received one nanocomposite hydrogel sample and one neat one (both in 0.5cm

x 1cm x 0.1cm dimensions). After 14 days, following an euthanasia treatment, the implantation sites were harvested. To assess the degradation level of the samples after implantation, we compared the size of the hydrogel implanted with its original size. For histological evaluations, the samples were fixed in a 4% paraformaldehyde solution and dehydrated by immersion into a 30% sucrose solution overnight. Later, three 40 μm sections were mounted on microscope slides and stained using hematoxylin and eosin (H&E) for analyzing the degree of tissue response, i.e. inflammation and fibrosis. The inflammation was characterized based upon the density of neutrophils, giant cells, and lymphocytes, and fibrosis was identified via the collagen deposition level. It is worthy to note that all the animal experiments were performed under the guidelines approved by the National Taiwan University, Animal Resource Center.

2.5.4. Statistical Analysis

One-way analysis of variance (ANOVA) was employed for statistical analysis of biological data. In this regard, the *p*-values smaller than 0.05 represented a significant difference between the compared data.

3. Results and discussion

3.1. Morphology and chemistry of the nanocomposite hydrogel

The weight average molecular weight (M_w) of the alginate sample, as determined by GPC, is as much as 186 kDalton with a polydispersity index of 1.135. Figure 2a shows the CD spectrum for the alginate used in our experiments. According to this graph, peak/trough ratio is less than one and ≈ 0.11. Thus, M/G can be calculated via the equation 1 and as much as 22%. The viscosity of the alginate solution raises from 2362 to 2937 cp as soon as inclusion of the CAGNFs, most likely due to higher alginate intermolecular interactions and cross-linking induced by presence of the nanofiller. The distribution mode of the nanofillers across a matrix is a vital factor that governs the uniform, isotropic structural and biological properties of the resulting nanocomposite system. The morphology of the CAGNFs before and after hybridization with alginate is seen in Figure 2b-e, respectively. According to the AFM images, Figure 2b, the nanofilaments are as long as several micrometers and as thin as around 250 nm. Optical microscopy images, Figure 2d&e, clearly witness the homogenous distribution of CAGNFs within the alginate matrix. This finding is indeed promising and can guarantee the isotropic interaction of cells with the samples' surface and also optimum structural properties of the nanocomposite. This mode of distribution reflects a proper bonding between the nanofilaments and polymer chains. This postulate was verified using ATR-FTIR, Figure 2f.

Comparing the IR graphs of alginate and CAGNF/alginate, it is evidently seen that almost all the characteristic peaks of alginate have been preserved while new peaks appear that are related to the nanofilaments and their functional groups. The peaks at 1300, 1720, and 1196 cm^{-1} represent -OH, C=O and C-O-C existing on the CAGNFs' surface, respectively(Fu et al., 2016). When the FTIR spectra for the alginate and CAGNF/alginate samples are precisely analyzed, it is seen that some characteristic peaks have shifted. Such peak shifts imply optimum interaction of the nanofilaments and the matrix through a secondary bonding, e.g. hydrogen bonding(S.Sh. Homaeigohar et al., 2012). For instance, the hydroxyl peak is transferred from 3453 to 3435 cm^{-1} after inclusion of the nanofilaments. The large carboxyl peak (the symmetric –COO- stretching vibration) at 1627 cm^{-1} also shifts to 1610 cm^{-1}. The bonding between the two main components of the nanocomposite can enhance the dispersion mode of the nanofilaments and thus mechanical stability of the nanocomposite made thereof. However, presence of the mentioned functional groups enabling the bonding, can decline conductivity of such nanofillers due to their electron withdrawing nature.

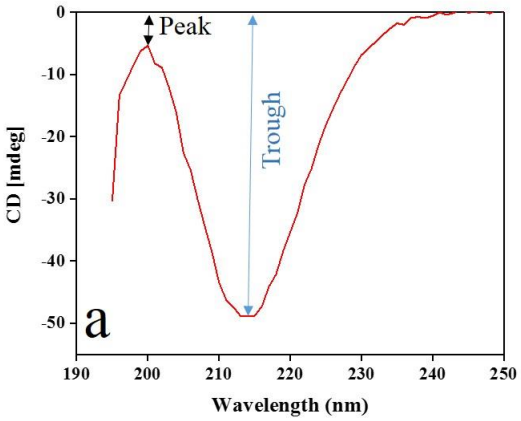

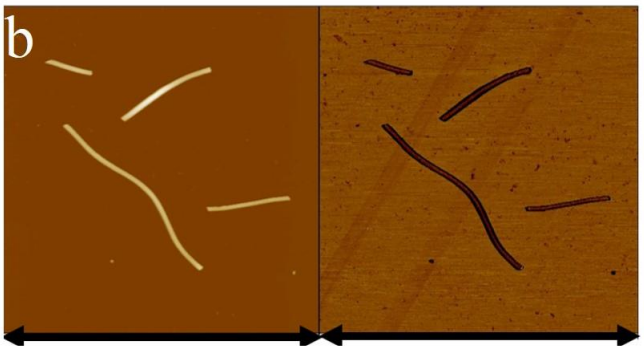

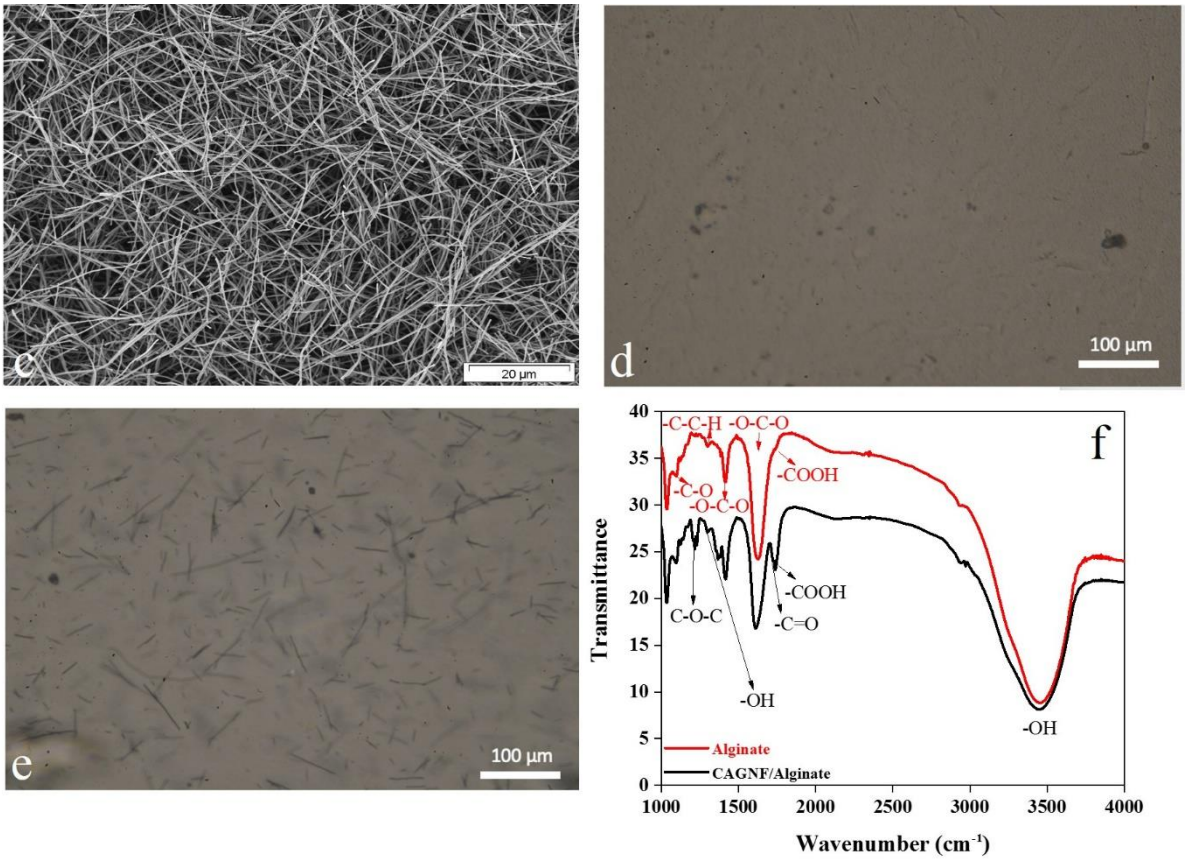

Figure 2. a) CD spectrum of sodium alginate solution at atmospheric pressure and room temperature. b) The AFM images show the dimensions of the CAGNFs (the black arrow represents 20 µm). c) The SEM micrograph demonstrates morphology of the as-synthesized CAGNFs. Optical microscopy images verify the uniform distribution of CAGNFs across the alginate matrix when comparing pure alginate's image (d) with CAGNF/alginate's (e). f) ATR-FTIR spectra for CAGNF/alginate and alginate. A precise analysis implies that there is a non-covalent bonding between CAGNFs and alginate molecules leading to their homogenous distribution. The peaks were identified according to (El-Houssiny et al., 2016; Fu et al., 2016).

To investigate the effect of inclusion of CAGNFs into alginate on the structural properties of the nanocomposite hydrogel, their mechanical and electrical properties were determined. Figure 3a shows that the CAGNF/alginate hydrogel possesses notably higher stiffness (elastic modulus) (56.14 Vs. 18.4 MPa) and maximum tensile strength (1.067 Vs. 0.378 MPa) compared to its neat counterpart. In terms of elongation, both the samples show an almost equal stretchability and flexibility (0.093). Toughness of the nanocomposite sample is also largely enhanced (≈3 times) versus that of the neat sample (0.07 Vs. 0.025 $MJ.m^{-3}$). The mechanical properties obtained for the nanocomposite hydrogel are quite promising when compared with those reported in other systems. For instance, Meng et al. (Meng et al., 2013) show that incorporation of carbon nanofibers (CNFs) into poly (2-hydroxyethyl methacrylate) (pHEMA, a biocompatible hydrogel) leads to a lower ultimate tensile strength (8.33 MPa) than

the neat hydrogel's (26.95 MPa). For a nanocomposite hydrogel system comprising carbon nanotube (CNT) and gelatin methacrylate (GelMA), an elastic modulus of 25 kPa has been reported (Shin et al., 2015) that is much lower than our nanocomposite's. In general, an elastic, flexible substrate material engenders a more optimum neurite extension. Cells apply tension on their underlying surface, specifically during migration. They recognize the surface's elasticity by their cellular receptors, mainly integrins, operating as mechanotransducers. When subjected to a highly stiff, or inelastic, material, the tension force required by the neurites for the sake of migration could be extremely large, hampering their extension. On the other hand, on a highly elastic substrate, even a low tension force applied by the neurites could give rise to attraction of the material towards the cell body rather than the neurite extending. Accordingly, a balance in terms of elasticity i.e. a desirable intermediate elasticity is necessary to largely drive the neurite extension (Gunn, Turner, & Mann, 2005). As will be shown later, the promising neurite outgrowth recorded in our study implies that the obtained elasticity for our materials lies in this optimum range that supports the neuron growth and development. The reason for the highly optimized mechanical properties of our nanocomposite hydrogel must be sought in the favorable interaction between CAGNFs and alginate. The likely esterification reaction between hydroxyl and carboxyl groups of CAGNFs and alginate and/or formation of a secondary (hydrogen) bonding between the components can stabilize the nanocomposite structure. Additionally, the calcium ions existing in the alginate matrix, can crosslink the nanofilaments and hydrogel molecules and lead to a higher mechanical stability of the nanocomposite hydrogels versus their neat counterpart. Other than the proper bonding between the CAGNFs and alginate matrix enabling an efficient load transfer from polymer to the nanofiller, the likely alignment of the nanofilaments during solidification can be also in charge of the improved mechanical properties (Kharaziha et al., 2014; Spinks et al., 2006). With respect to toughness, slippage at the CAGNF-alginate interface leads to a larger energy absorption while loading thus to a higher toughness for the nanocomposite hydrogel (Salvetat-Delmotte & Rubio, 2002).

Figure 3b compares the electrical conductivity of the nanocomposite hydrogel versus that of the neat one. It is worthy to note that the electrical conductivity of the CAGNFs was measured as much as $\approx$ 2 S. cm^{-1}, that is significantly higher than that of the hydrogels. Surprisingly, the nanocomposite hydrogel shows a lower conductivity that could be attributed to formation of large voids within the structure. The voids are resulted from the extensive interaction of the nanofilaments and the encapsulating polymer and thus accumulation of polymer chains around the CAGNFs, as schematically demonstrated in Figure 3c. To validate

this assumption, we measured the swelling percentage of the neat and nanocomposite samples when immersed in PBS for a given time and weighed. Figure 3d shows that the nanocomposite hydrogel has a higher swelling percentage thanks to the presence of large voids. Such voids decline the conductivity and act as insulators within the hydrogels. The measured porosity values (Figure 3e) also verify this assumption. A similar observation has been reported by Liu et al.(X. Liu et al., 2016). They state that while a neat hydrogel of oligo(polyethylene glycol fumarate) (OPF) possesses totally solidified internal layers, the nanocomposite hydrogel made thereof and containing carbon nanomaterials (graphene oxide-carbon nanotube) shows a highly rough, tubular structure. However, in their system the carbon nanofillers form an integrated, continuous conductive network and raise the conductivity notably from $2x10^{-4}$ $S.m^{-1}$ up to $80x10^{-4}$ $S.m^{-1}$. In contrast, in our material, a non-percolating network of CAGNFs is unable to increase conductivity, while the insulating voids lower the bulk electrical conductivity of the nanocomposite hydrogel. If we resemble the hydrogels to a closed-cell conductive foam, the electrical conductivity (σ_{dc}) can be correlated to the porosity value (θ), as explained by Liu et al. (equation 7):(Chand & Sharma, 2012; P. Liu, Li, & Fu, 1999)

$$\sigma_{dc} = \left[\frac{a(1-\theta)}{(1-0.121)(1-\theta)^{1/2}}\right] \quad (7)$$

the factor *a* is a constant that depends on the structure of the porous material. However, considering the poor conductivity of alginate, a model based on polymeric foams could be more relevant, as widely studied by Chand and Sharma(Chand & Sharma, 2012). They relate the electrical conductivity of a polymeric foam to its porosity through the following equation (8):

$$\sigma_{dc} = \frac{\alpha(1-\theta)}{(1-\theta)^{s}} \quad (8)$$

where *s* is a factor that is porosity and thickness (*t*) dependent and can be determined as $s=(1-t)+(1-\theta)$.

The two abovementioned models both certify that increase of porosity, as observed in our system after incorporation of the CAGNFs into alginate, leads to loss of electrical conductivity. Despite this reality, an improved mechanical stability along with presence of locally conductive surface domains wherein the CAGNFs are located could be promising for the biological activity of the nerve cells seeded on the nanocomposite hydrogel. In fact, one of the most important challenges the conventional scaffolds encounter is that they are unable to provide a platform wherein intercellular communication is allowed(Dozois, Bahlmann, Zilberman, & Tang, 2017). Here, presence of the conductive CAGNFs is assumed to enable the cells contact, leading to their enhanced proliferation, growth, and colonization.

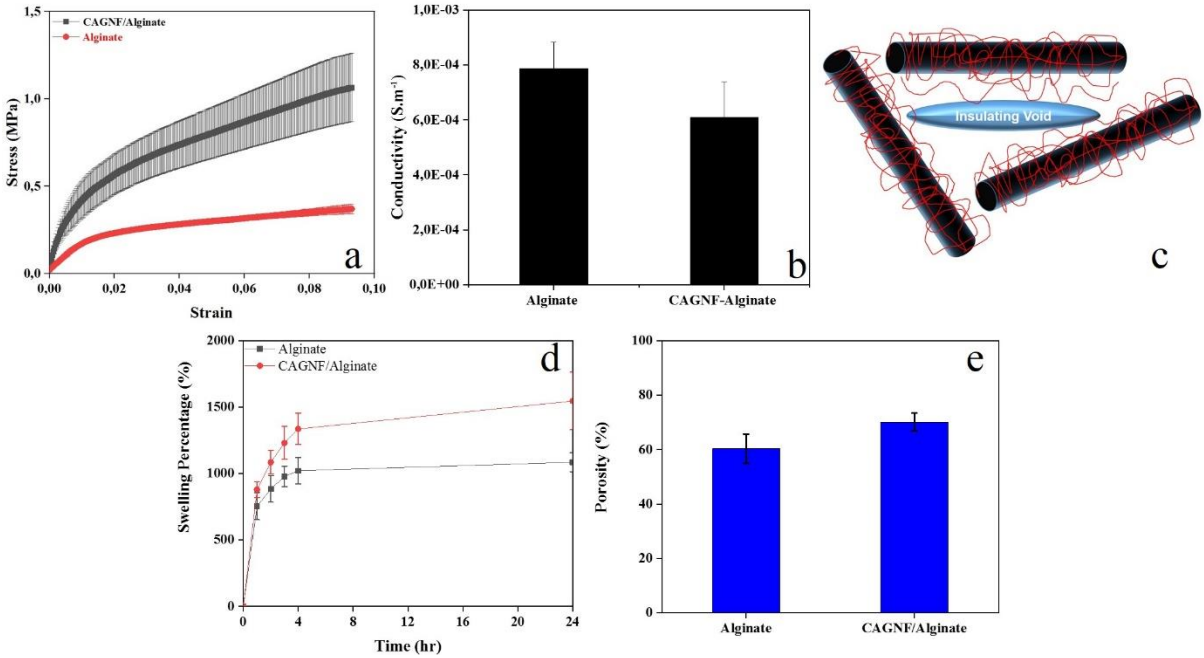

Figure 3. a) The stress-strain graph shows different mechanical features of the hydrogel samples (n: the number of the tested samples was 5 and the error bars calculated using the standard deviation (s.d.) function of the Origin software indicate the corresponding s.d.'s). b) Electrical conductivity of the neat and nanocomposite hydrogel samples (n= 5). c) Schematic illustration of the formation of insulating voids that are assumed to be responsible for the lower conductivity observed in the nanocomposite hydrogel versus the neat one. The swelling (d) and porosity (e) percentage of the nanocomposite hydrogel compared to the neat one (n= 4).

To characterize the biocompatibility of the nanocomposite hydrogel developed in this study, each component should be evaluated separately and collectively. Alginate is a well-known biomaterial that has been suggested for a diverse range of medical applications. But, the CAGNFs as a nanofiller for the alginate based nanocomposites must be challenged with respect to biocompatibility. In this regard, CA functionalization is assumed to raise biocompatibility of the nanofilaments. Kagan et al.(Kagan et al., 2010) have reported that carboxylic based functionalization of carbon nanotubes (CNTs) can facilitate their enzymatic degradation into non-inflammatory products. In our study, we tracked the effect of functionalization on the biological interaction of cells (i.e. MSCs) with the graphite nanofilaments. Figure 4a compares the cytotoxicity effect of the CAGNFs with that of the GNFs with no particular functionality. Other than the first day, in the other days, there is a significant difference (p<0.05) in viability of MSCs in control (TCPS) with that of those next to GNFs. After the 3rd day, such a significant difference is observed between the MSCs present in the proximity of CAGNFs with those co-cultured with GNFs. Also, Figure 4b, the images taken after different time intervals from the cell cultures, implies a better biocompatibility of

the functionalized GNFs. Evidently, the MSCs are no longer alive and active next to the GNFs after 5 days, while in adjacent to the CAGNFs, they are proliferated as much as are they in the control medium after this duration. Supplementary videos 1&2 demonstrate the interaction of MSCs with the GNFs and CAGNFs, respectively. The origin of the cytotoxicity induced by the nanofilaments is not completely known and assumed to be linked to generation of reactive oxygen species (ROSs). Size, shape, and chemistry of the nanofilaments would strongly affect their toxic potential. In general, enzymatic biodegradation of the carboxylated nanofilaments (Kagan et al., 2010) and thus formation of smaller nanofilaments with larger surface defect density and higher electron donor–acceptor impurities raise ROS generation.(Elbahri et al., 2017) On the other hand, as Lyublinskaya et al.(Lyublinskaya et al., 2015) reported the higher the intracellular basal ROS level is, the larger the proliferation rate would be in the MSC cultures. In contrast, when the ROS level declines due to presence of antioxidant materials such as non-functionalized GNFs, the MSC proliferation is hampered.

The proliferation rate of the PC12 cells and cytotoxicity effect of the nanocomposite hydrogel were probed via the WST assay after 1, 4, and 7 days co-culturing of the cells and samples. The proliferation rate of the cells next to the nanocomposite hydrogel was evaluated against that with pure alginate and TCPS. Figure 5a shows that the nanocomposite hydrogel is able to preserve the normal proliferation rate of the cells.

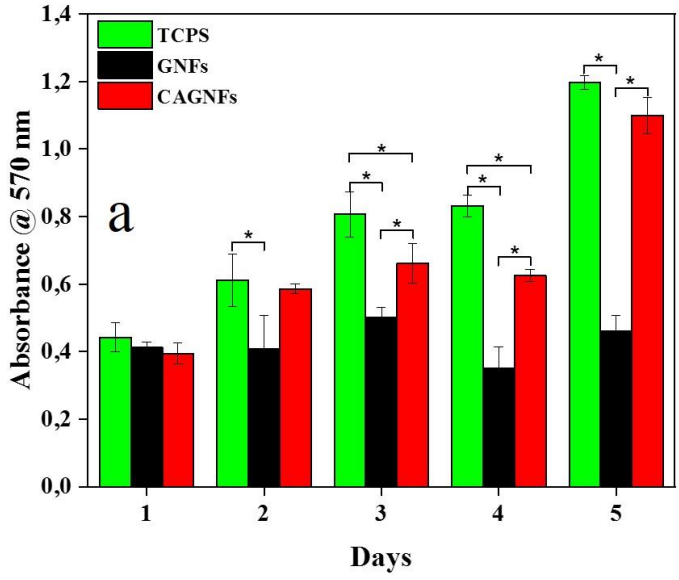

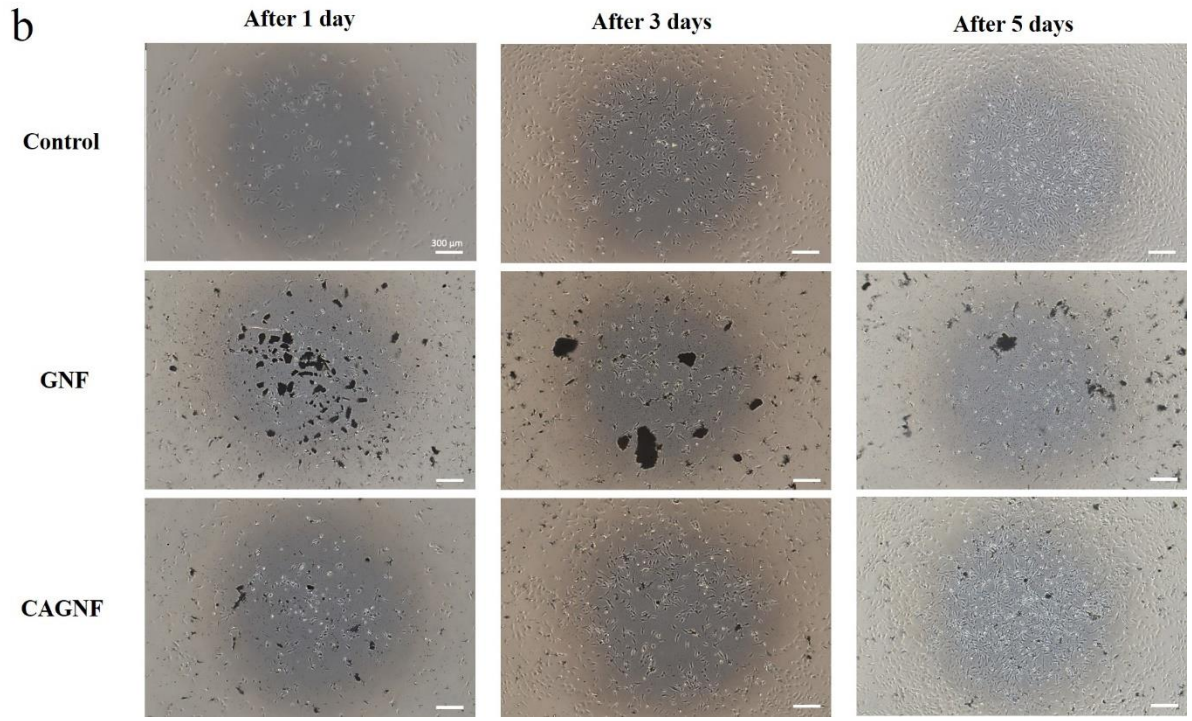

Figure 4. a) Cytotoxicity effect of the non-functionalized GNFs versus that of the CAGNFs. The results are shown as mean values ± s.d. (*$p < 0.05$ indicates a significant difference and the error bars represent standard deviations (s.d.). b) The cell-nanofilaments interaction after different intervals (note that large clusters of hydrophobic GNFs are clearly seen in the cell cultures, the middle row) (the scale bars represent 300 µm).

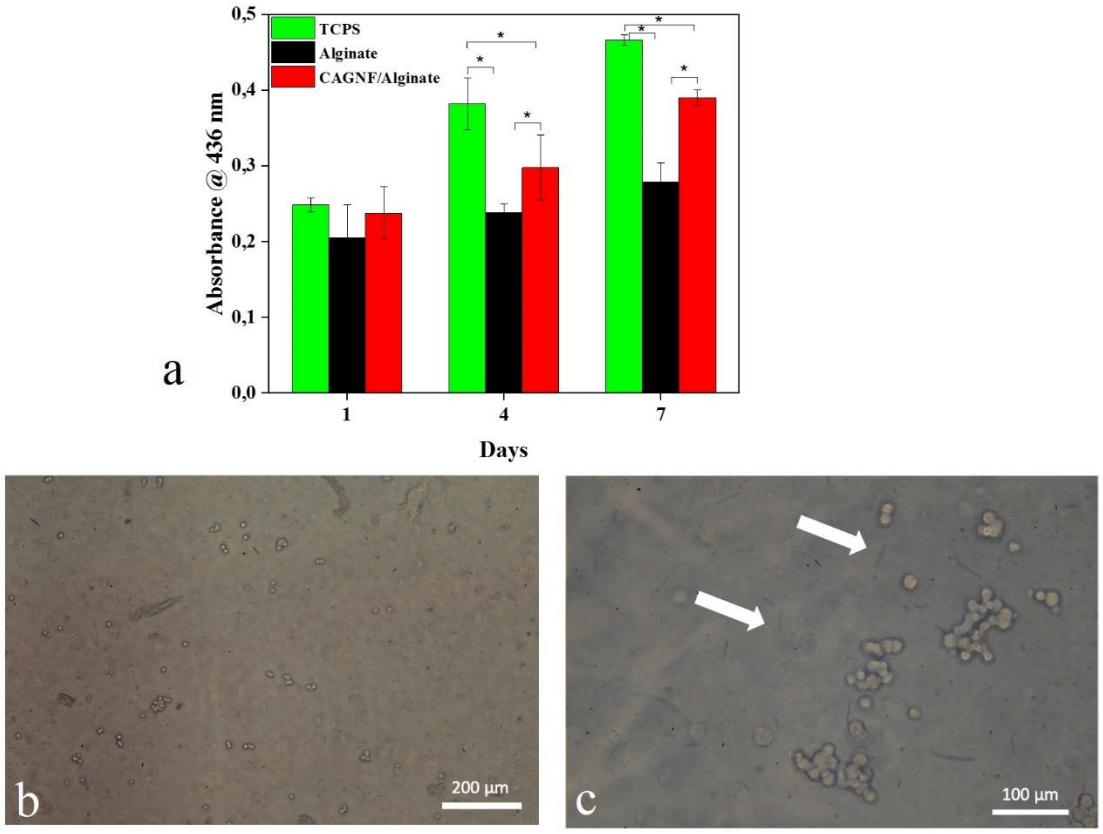

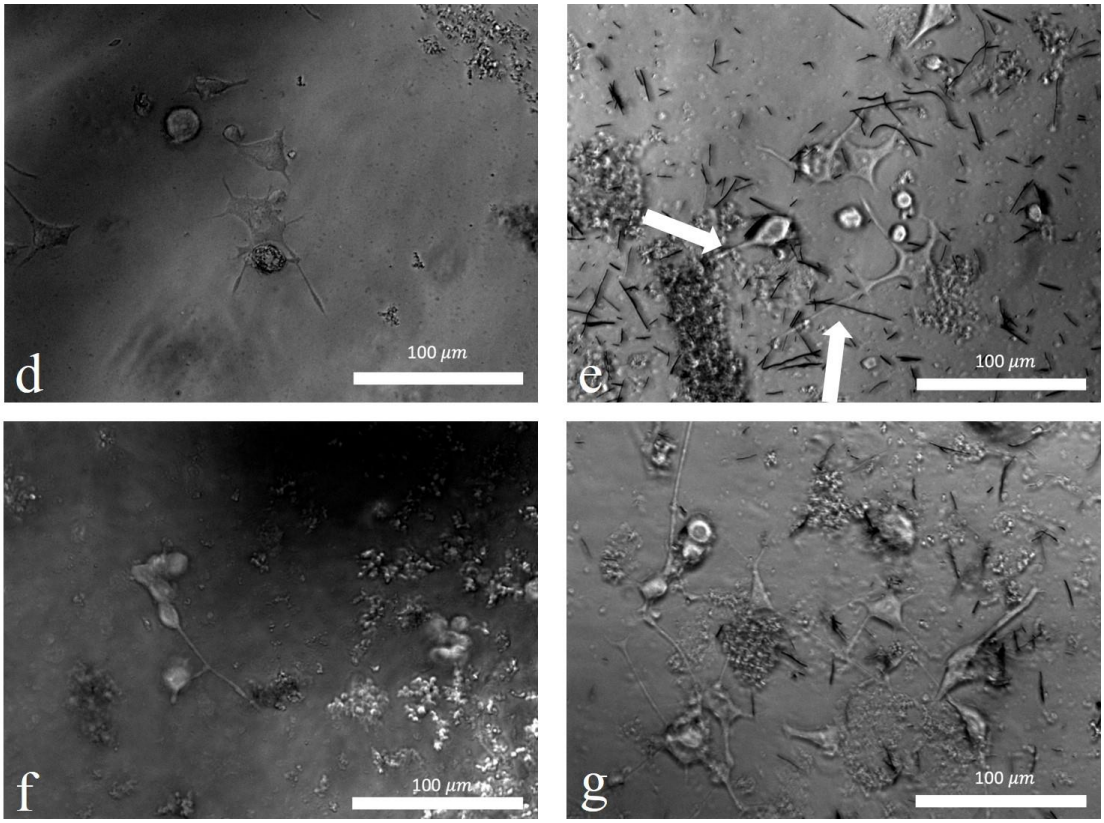

Figure 5. a) Cytotoxicity effect (represented by the WST absorbance at 436 nm) of the nanocomposite hydrogel (CAGNF/alginate) versus that of the neat alginate and TCPS. The results are shown as mean values ± s.d. (*$p < 0.05$ indicates a significant difference and the error bars represent standard deviations (s.d.). b) Sparse distribution of the PC12 cells on the surface of alginate compared to c) their colonization on the surface of the CAGNF/alginate sample, particularly, wherein the CAGNFs are present (marked by arrows) and enable electrical signaling and intercellular communication. d) A significant neurite outgrowth (marked by arrows) is observed on the surface of CAGNF/alginate (e&g: after 5 and 8 days, respectively) versus that on the alginate surface (d&f: after 5 and 8 days, respectively).

Among the studied samples, TCPS offers the highest cell proliferation rate, followed by the nanocomposite hydrogel. There is a significant difference ($p<0.05$) in the proliferation rate of the cells next to alginate with that in the proximity of the nanocomposite. Such a result implies that the nanocomposite hydrogel is sufficiently biocompatible and can induce cell proliferation. Figure 5b&c shows that there is a colonization taking place on the nanocomposite surface, while the cells are sparsely distributed on the alginate surface. In terms of number, the images clearly verify the WST assay result, Figure 5a. The negligible adhesion (number) of the cells on alginate, that inherently lacks mammalian cells adhesivity, could be attributed to two factors. First, the surface topography of alginate mimics the extracellular matrix and can drive cellular adhesion (K. Y. Lee & Mooney, 2012). Second, likely physical adsorption of cell adhesion molecules from adjacent fluids induced by a thermodynamic driving force could help

the cells stick to the surface (Rowley, Madlambayan, & Mooney, 1999). The subsequent cell-cell interactions further facilitate the aggregation of cells. The colonization of the cells on specific areas, where most likely are rich of conductive CAGNFs, imply that the local conductivity facilitates electrical signaling and communication of the cells and provides them with a better substrate for proliferation and growth. Also, the neurite outgrowth can be clearly observed for the cells seeded on the nanocomposite surface after 5 (Figure 5e) and 8 days (Figure 5g) co-culturing. Figure 5d&f illustrates the neurite expansion on the alginate surface that is notably less evident than that on the nanocomposite surface. In fact, the cells on the nanocomposite are richer in terms of the developed, long neurites that stem from the main cell body. Thus, thanks to its local conductive zones, the CAGNF/alginate offers a much better platform for the growth and differentiation of the nerve cells compared to alginate.(X. Liu et al., 2016) We also employed a staining assay to visualize the cell morphology on the hydrogel surfaces. After incubation for 5 days, the live cells were stained by rhodamine−phalloidin (RP, red) and DAPI to visualize F-actin arrangement and the cell nuclei, respectively. Figure 6a, i.e. the merged image of the two components, demonstrates that both the hydrogels of neat and nanocomposite help the cells survive, yet with a more notable impact by the nanocomposite. These images show not only the cell morphologies but also the neurite outgrowth for the cells seeded on the hydrogels that is notably more evident for the nanocomposite, as highlighted by the metamorph images, as well. Clearly, the area covered by the cells on the nanocomposite hydrogel is extensively larger than that on the neat counterpart. Based on such images, the neurite length and the PC12 cell expansion area of almost 50 cells were measured by the ImageJ Software. Additionally, the percent of the cells with neurite was quantified. Figure 6b&c shows that compared to the neat hydrogel, a larger population of the cells with neurite exists on the nanocomposite hydrogels (64% Vs. 41%) and the neurite bearing cells on the surface of the nanocomposite hydrogel possess significantly longer neurites (195 Vs. 53 μm). While the enhanced surface roughness and partial hydrophobicity due to the presence of the graphitic nanofilaments, thereby promoted serum protein adsorption, play a supportive role, this performance is mainly attributed to the local conductive surface zones. Such regions allow for cell communication and stimulate the neural differentiation of the PC12 cells. A similar behavior has been reported by Liu et al.(X. Liu et al., 2017) for the conductive rGO_aCNT_{pega}-OPF-MTAC hydrogel versus the neutral OPF hydrogel. Figure 6d shows that the cells on alginate spread insignificantly and cover a limited area of $\approx 20 \times 10^3$ μm^2. In contrast, on the conductive nanocomposite hydrogel, spreading of the cells is more notable and as much as $\approx 34 \times 10^3$ μm^2. The reason for the totally different interaction mode and thus larger stimulation

of the PC12 cells on the nanocomposite hydrogel compared to the neat one should be sought in their electromechanical characteristics. On the alginate sample, the PC12 cells are unable to adhere to the surface and thus spread less notably due to insufficient cell-sample interaction. The alginate chains are negatively charged and repel the negatively charged cells and also there is a low mechanical support (roughness) on the surface when compared with the nanocomposite hydrogel. With respect to the former factor, it is worthy to note that the PC12 cells show different magnitudes of phosphatidylserine (PS) exposure at the external membrane leaflet and whereby achieving a negative charge.(Tsai, Hung, Liu, Chen, & Pan, 2012) This same surface charge between alginate and the PC12 cells does not let them approach the sample. In contrast, the rougher and stiffer surface of the nanocomposite hydrogel enables the cells to stick to the surface and spread and enjoy of the conductive channels beneath them that provide them with the intercellular signaling possibility. This facility encourages the cells to adhere, spread, proliferate, and differentiate onto the nanocomposite sample. Figure 7 clearly witnesses that the cells after 14 days seeding onto the nanocomposite hydrogel spread and the grown neurites and axons are almost interconnected. Formation of this network of neural cells is extremely promising and indicates the high potential of the nanocomposite hydrogel for neural tissue engineering.

The *in vivo* degradation rate of the hydrogel samples with and without presence of the CAGNFs and also their likely inflammatory response were characterized via implantation of the samples in the body of animal (guinea pig) models. As shown in Figure 8a, after 7 days, the hydrogel samples are in a comparable size with their primary states but after 14 days implantation, they are biodegraded significantly. Gradual release of Ca^{2+} into the surrounding media driven by the exchange reactions with monovalent cations e.g. Na^{+} engenders the *in vivo* degradation of alginate (K. Y. Lee & Mooney, 2012). The biodegradation rate is more notable for the neat sample, while the nanocomposite one seems crushed and sparse. Such an *in vivo* degradation behavior for the hydrogel implants is quite promising for healing and regeneration of the tissues(Fan, Fu, Zhu, & Wang, 2016; Mehdizadeh, Weng, Gyawali, Tang, & Yang, 2012). Figure 8b witnesses that there is no particular reddening and inflammation in the skin of the animal model after 14 days implantation of both the hydrogel samples. To ascertain of the biocompatibility of the nanocomposite hydrogel and its degradation products, the histological sections of the tissues located around the implant were stained with H&E. Figure 8c shows that after 7 days, many neutrophils i.e. inflammatory cells, represented by the dark blue (purple) spots, are present in the studied tissues. These cells originated from blood vessels are indicative of the moderate acute inflammatory response. Such an observation has been

previously reported by Fan et al.(Fan et al., 2016), as well and attributed to the surgical wounding. This assumption could be valid in case alginate's response is similar, that is the case.

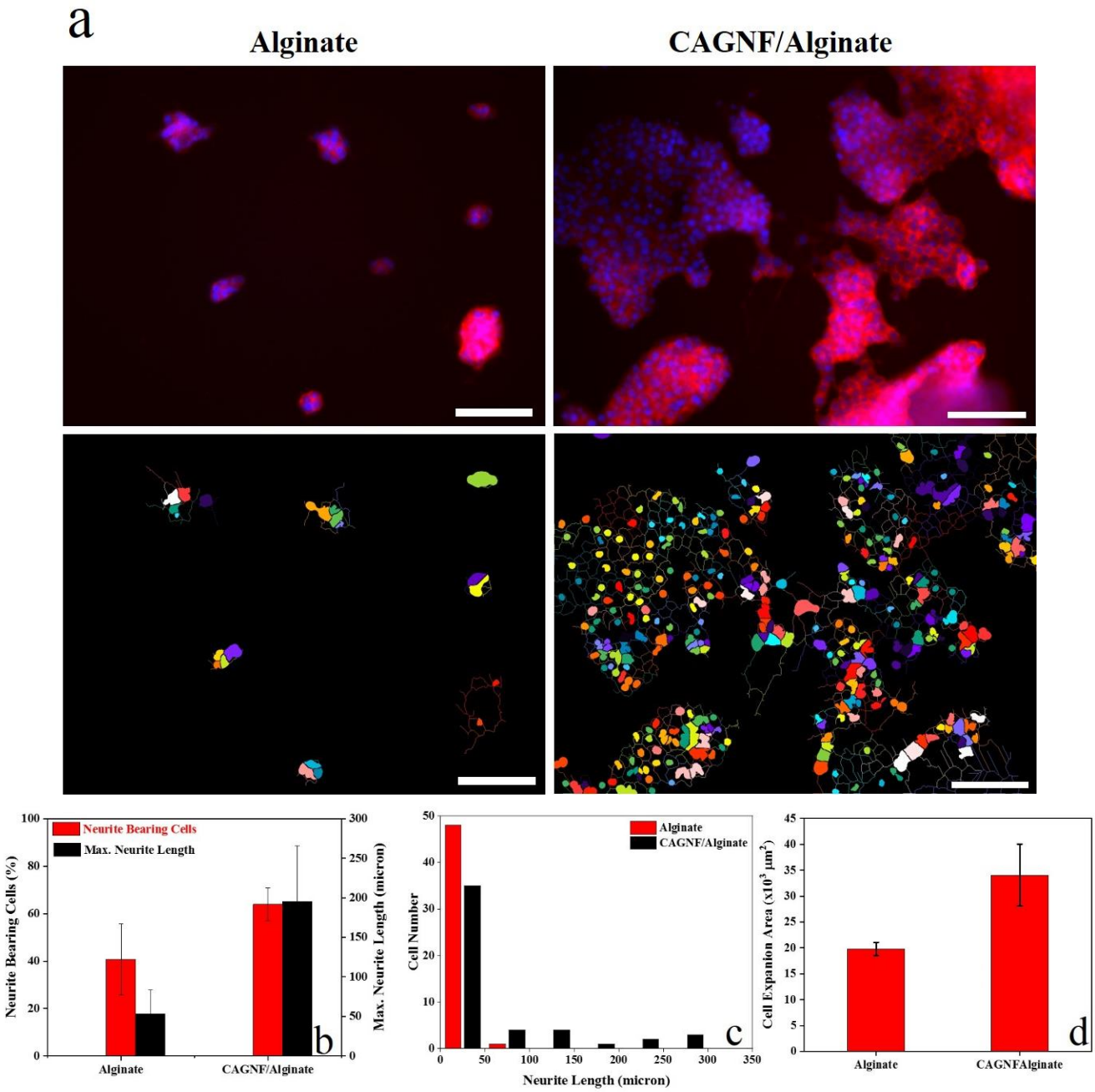

Figure 6. a) Merged fluorescent (cellular F-actin (red) and nuclei (blue)) images of PC12 cells seeded on alginate and CAGNF/alginate after 5 days (the upper row) and the Metamorph images indicating population of the PC12 cells on each sample, cell morphologies as well as the number of the cells with neurites (the lower row) (scale bars represent 100 µm). b) The population of the neurite bearing cells found on the surface of alginate and CAGNF/alginate along with the calculated maximum neurite length of such cells. c) Histogram of the neurite length distribution for the cells differentiated onto the alginate and CAGNF/alginate samples. d) The cellular spreading area calculated based on 50 randomly selected cells seeded onto the hydrogel samples after 4 days.

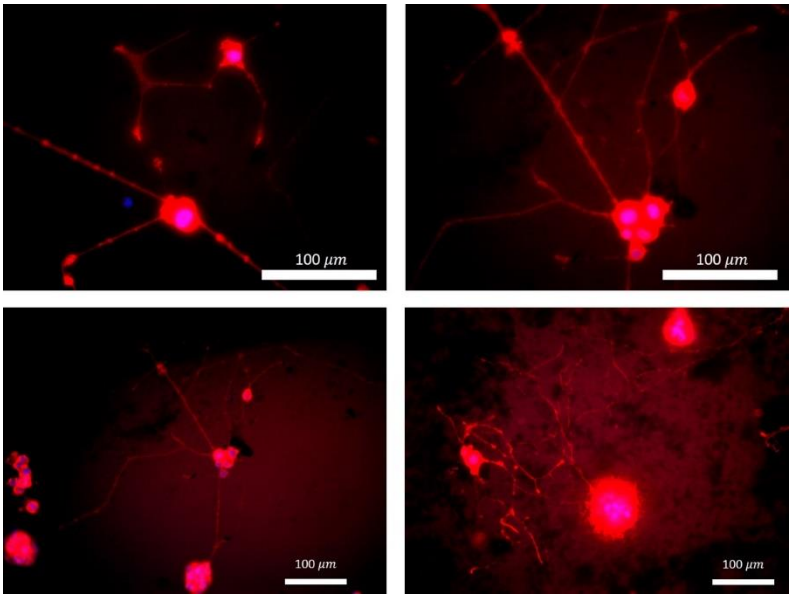

Figure 7. Neurite network formed after 14 days co-culturing of the PC12 cells with the nanocomposite hydrogel stressing suitability of the material for neural tissue engineering and regeneration of a damaged nerve connection (Upper row: 400x and lower row: 200x).

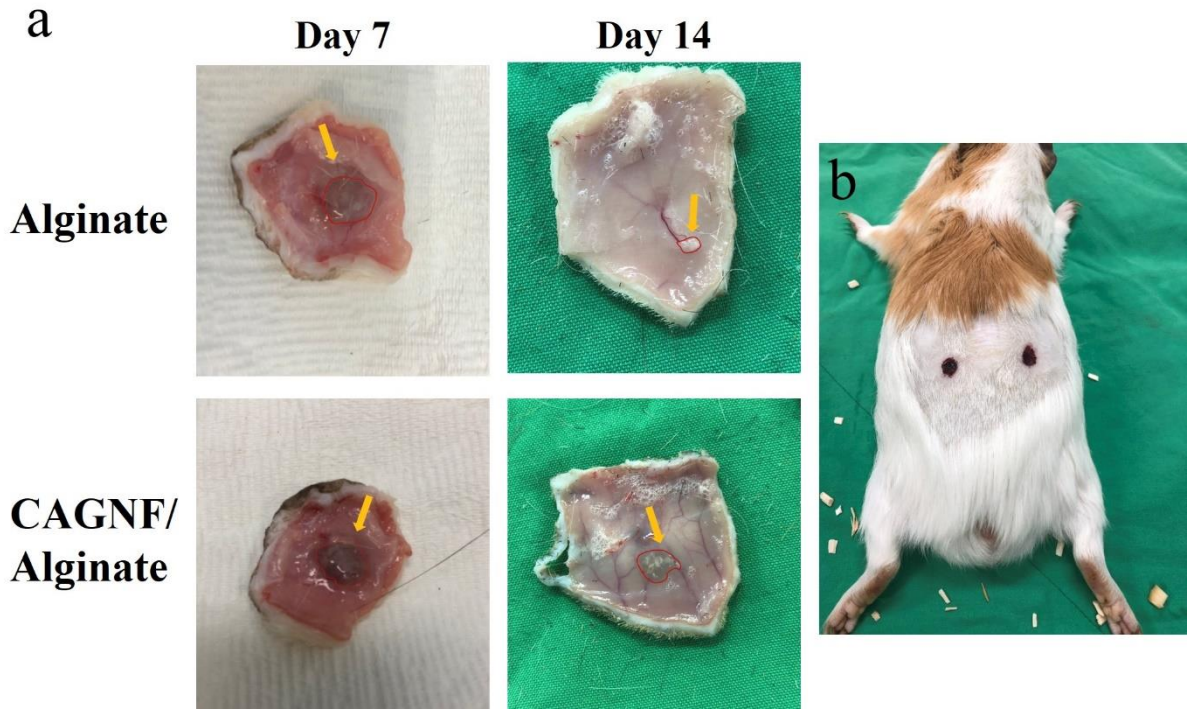

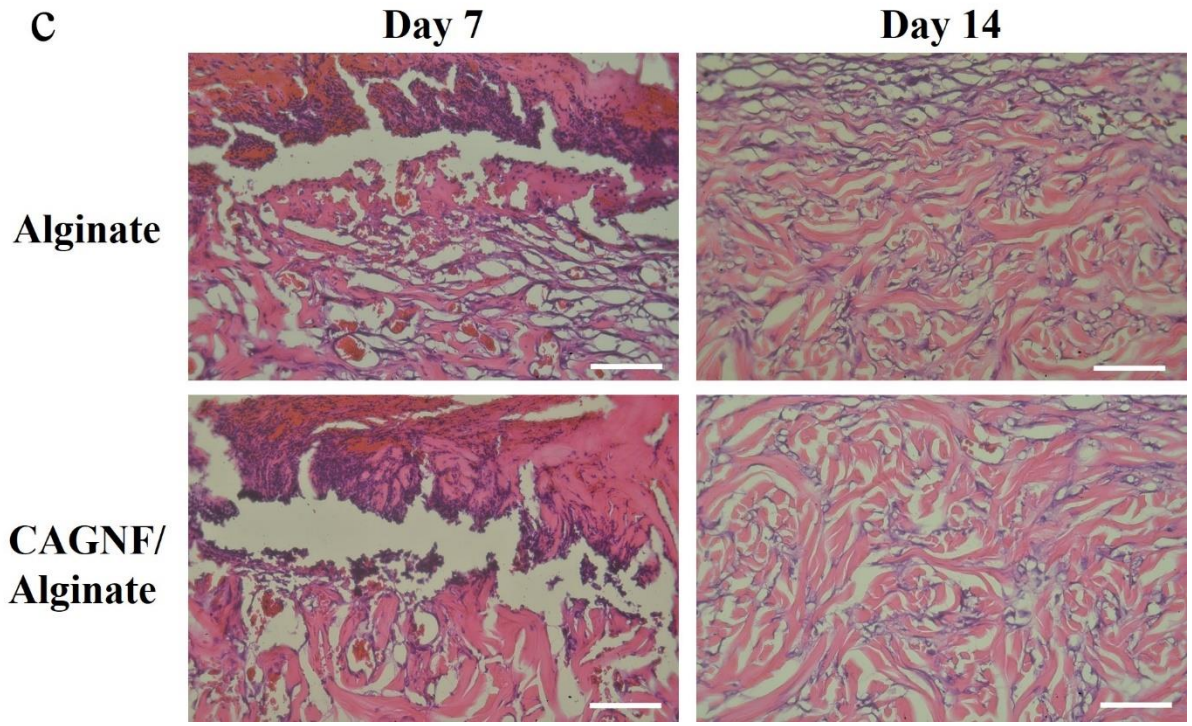

Figure 8. a) Camera images of the hydrogel implants (embedded within the guinea pig's skins) harvested on day 7 and 14. The arrows mark the samples, for a better identification. Obviously, both the samples have been biodegraded after 14 days with a lower degradation rate for the nanocomposite hydrogel. The inflammated red tissues (day 7) turn to non-inflammated, white ones (day 14) over time. b) The area surrounding the implantation sites for the alginate and CAGNF/alginate samples show no particular reddening and inflammation, implying a comparable *in vivo* performance for both the samples after 14 days. c) H&E staining of the tissues encompassing the hydrogel implants after 7 and 14 days implantation; clearly the density of neutrophils (dark purple dots) decline over time and a comparable inflammatory response is deduced for both the alginate and CAGNF/alginate samples (scale bar represents 100 μm).

After 14 days, the number of the inflammatory cells notably decline, as seen in Figure 8c. This behavior implies that the inflammatory reaction in response to the presence of the implant and its degradation products has been alleviated.(Fan et al., 2016) Moreover, during the entire 14 day implantation, no giant cells reaction and fibrosis was recorded within the tissues. Again absence of such adverse reactions stresses the biocompatibility of the nanocomposite hydrogel. Interestingly, the nanocomposite hydrogel demonstrates a comparable in vivo performance with alginate. Given the fame and wide applicability of alginate as a natural biomaterial in biomedicine, a promising potential for the nanocomposite hydrogel can be foreseen. Particularly, when a lower degradation rate, higher robustness, and local conductivity of this new kind of hydrogel scaffold is recalled.

4. Conclusion

In this study, we validated that the graphite nanofilaments, greenly functionalized simply by citric acid, are notably adapted with an alginate hydrogel and uniformly dispersed therein. By employing such eco-friendly, novel functional carbon nanofillers, the hydrogel nanocomposite offers local conductive zones, enabling intercellular signaling and provoking cells responses, and a robust structure with a low degradation rate.

In vitro tests witnessed the optimum biocompatibility of both the nanofiller and the nanocomposite made thereof. A remarkable biological behavior in terms of proliferation and differentiation was recorded for the cells co-cultured with the nanocomposite hydrogels. *In vivo* test also stressed biocompatibility of the nanocomposite, given no notable inflammatory response in the hosting tissue of animal models. On the whole, the collected results confidently imply the optimum applicability of the CAGNF/alginate nanocomposite for neural tissue engineering applications.

Acknowledgement

S.H. would like to acknowledge the financial support received from the Academy of Finland (Grant No. 314947). The authors also thank Hao-Ying Hsieh and Yu-Hsin Wang for their precious consultation and contribution during the *in vivo* and *in vitro* studies, respectively.

References

Brett Runge, M., Dadsetan, M., Baltrusaitis, J., Knight, A. M., Ruesink, T., Lazcano, E. A., . . . Yaszemski, M. J. (2010). The development of electrically conductive polycaprolactone fumarate–polypyrrole composite materials for nerve regeneration. *Biomaterials, 31*(23), 5916-5926. doi:https://doi.org/10.1016/j.biomaterials.2010.04.012

Chand, N., & Sharma, J. (2012). Influence of porosity on resistivity of polypropylene foams. *Journal of Cellular Plastics, 48*(1), 43-52.

Ding, T., Lu, W. W., Zheng, Y., Li, Z. y., Pan, H. b., & Luo, Z. (2011). Rapid repair of rat sciatic nerve injury using a nanosilver-embedded collagen scaffold coated with laminin and fibronectin. *Regenerative medicine, 6*(4), 437-447.

Dozois, M. D., Bahlmann, L. C., Zilberman, Y., & Tang, X. S. (2017). Carbon nanomaterial-enhanced scaffolds for the creation of cardiac tissue constructs: A new frontier in cardiac tissue engineering. *Carbon, 120*, 338-349.

El-Houssiny, A., Ward, A., Mostafa, D., Abd-El-Messieh, S., Abdel-Nour, K., Darwish, M., & Khalil, W. (2016). Drug–polymer interaction between glucosamine sulfate and alginate nanoparticles: FTIR, DSC and dielectric spectroscopy studies. *Advances in Natural Sciences: Nanoscience and Nanotechnology, 7*(2), 025014.

Elbahri, M., Abdelaziz, R., Disci-Zayed, D., Homaeigohar, S., Sosna, J., Adam, D., . . . Abdelaziz, M. (2017). Underwater Leidenfrost nanochemistry for creation of size-tailored zinc peroxide cancer nanotherapeutics. *Nature communications, 8*.

Fan, C., Fu, J., Zhu, W., & Wang, D.-A. (2016). A mussel-inspired double-crosslinked tissue adhesive intended for internal medical use. *Acta Biomaterialia, 33*, 51-63.

Florea-Spiroiu, M., Bala, D., Balan, A., Nichita, C., & Stamatin, I. (2012). Alginate matrices prepared in sub and supercritical CO2. *Digest Journal of Nanomaterials and Biostructures, 7*, 1549-1555.

Frost, H. K., Andersson, T., Johansson, S., Englund-Johansson, U., Ekström, P., Dahlin, L. B., & Johansson, F. (2018). Electrospun nerve guide conduits have the potential to bridge peripheral nerve injuries in vivo. *Scientific reports, 8*(1), 16716.

Fu, Q., Wang, X., Si, Y., Liu, L., Yu, J., & Ding, B. (2016). Scalable Fabrication of Electrospun Nanofibrous Membranes Functionalized with Citric Acid for High-Performance Protein Adsorption. *ACS applied materials & interfaces, 8*(18), 11819-11829. doi:10.1021/acsami.6b03107

Golafshan, N., Gharibi, H., Kharaziha, M., & Fathi, M. (2017). A facile one-step strategy for development of a double network fibrous scaffold for nerve tissue engineering. *Biofabrication, 9*(2), 025008.

Golafshan, N., Kharaziha, M., & Fathi, M. (2017). Tough and conductive hybrid graphene-PVA: Alginate fibrous scaffolds for engineering neural construct. *Carbon, 111*, 752-763. doi:https://doi.org/10.1016/j.carbon.2016.10.042

Griffin, J. W., Hogan, M. V., Chhabra, A. B., & Deal, D. N. (2013). Peripheral nerve repair and reconstruction. *JBJS, 95*(23), 2144-2151.

Guarino, V., Altobelli, R., della Sala, F., Borzacchiello, A., & Ambrosio, L. (2018). Alginate Processing Routes to Fabricate Bioinspired Platforms for Tissue Engineering and Drug Delivery *Alginates and Their Biomedical Applications* (pp. 101-120): Springer.

Gunn, J. W., Turner, S. D., & Mann, B. K. (2005). Adhesive and mechanical properties of hydrogels influence neurite extension. *Journal of Biomedical Materials Research Part A, 72A*(1), 91-97. doi:10.1002/jbm.a.30203

Hashimoto, T., Suzuki, Y., Suzuki, K., Nakashima, T., Tanihara, M., & Ide, C. (2005). Review Peripheral nerve regeneration using non-tubular alginate gel crosslinked with covalent bonds. *Journal of Materials Science: Materials in Medicine, 16*(6), 503-509.

Homaeigohar, S., Dai, T., & Elbahri, M. (2013). Biofunctionalized nanofibrous membranes as super separators of protein and enzyme from water. *Journal of colloid and interface science, 406*(0), 86-93. doi:http://dx.doi.org/10.1016/j.jcis.2013.05.076

Homaeigohar, S., & Elbahri, M. (2019). An Amphiphilic, Graphitic Buckypaper Capturing Enzyme Biomolecules from Water. *Water, 11*(1), 2.

Homaeigohar, S., Strunskus, T., Strobel, J., Kienle, L., & Elbahri, M. (2018). A Flexible Oxygenated Carbographite Nanofilamentous Buckypaper as an Amphiphilic Membrane. *Advanced Materials Interfaces, 5*(8), 1800001. doi:doi:10.1002/admi.201800001

Homaeigohar, S. S., Sadi, A. Y., Javadpour, J., & Khavandi, A. (2006). The effect of reinforcement volume fraction and particle size on the mechanical properties of β-tricalcium phosphate–high density polyethylene composites. *Journal of the European Ceramic Society, 26*(3), 273-278. doi:https://doi.org/10.1016/j.jeurceramsoc.2004.10.003

Homaeigohar, S. S., Shokrgozar, M. A., Sadi, A. Y., Khavandi, A., Javadpour, J., & Hosseinalipour, M. (2005). In vitro evaluation of biocompatibility of beta-tricalcium phosphate-reinforced high-density polyethylene; an orthopedic composite. *Journal of Biomedical Materials Research Part A, 75A*(1), 14-22. doi:10.1002/jbm.a.30333

Kagan, V. E., Konduru, N. V., Feng, W., Allen, B. L., Conroy, J., Volkov, Y., . . . Kapralov, A. (2010). Carbon nanotubes degraded by neutrophil myeloperoxidase induce less pulmonary inflammation. *Nature nanotechnology, 5*(5), 354.

Kehoe, S., Zhang, X., & Boyd, D. (2012). FDA approved guidance conduits and wraps for peripheral nerve injury: a review of materials and efficacy. *Injury, 43*(5), 553-572.

Kharaziha, M., Shin, S. R., Nikkhah, M., Topkaya, S. N., Masoumi, N., Annabi, N., . . . Khademhosseini, A. (2014). Tough and flexible CNT–polymeric hybrid scaffolds for engineering cardiac constructs. *Biomaterials, 35*(26), 7346-7354.

Kim, M. S., & Kim, G. (2014). Three-dimensional electrospun polycaprolactone (PCL)/alginate hybrid composite scaffolds. *Carbohydrate Polymers, 114*, 213-221. doi:https://doi.org/10.1016/j.carbpol.2014.08.008

Lee, J. H., Lee, J.-Y., Yang, S. H., Lee, E.-J., & Kim, H.-W. (2014). Carbon nanotube–collagen three-dimensional culture of mesenchymal stem cells promotes expression of neural phenotypes and secretion of neurotrophic factors. *Acta Biomaterialia, 10*(10), 4425-4436.

Lee, K. Y., & Mooney, D. J. (2012). Alginate: Properties and biomedical applications. *Progress in polymer science, 37*(1), 106-126. doi:https://doi.org/10.1016/j.progpolymsci.2011.06.003

Li, R., Liu, Z., Pan, Y., Chen, L., Zhang, Z., & Lu, L. (2014). Peripheral nerve injuries treatment: a systematic review. *Cell biochemistry and biophysics, 68*(3), 449-454.

Lin, Y.-L., Jen, J.-C., Hsu, S.-h., & Chiu, M. (2008). Sciatic nerve repair by microgrooved nerve conduits made of chitosan-gold nanocomposites. *Surgical neurology, 70*, S9-S18.

Liu, P., Li, T., & Fu, C. (1999). Relationship between electrical resistivity and porosity for porous metals. *Materials Science and Engineering: A, 268*(1-2), 208-215.

Liu, X., Miller, A. L., Park, S., Waletzki, B. E., Zhou, Z., Terzic, A., & Lu, L. (2017). Functionalized carbon nanotube and graphene oxide embedded electrically conductive hydrogel synergistically stimulates nerve cell differentiation. *ACS applied materials & interfaces, 9*(17), 14677-14690.

Liu, X., Miller II, A. L., Park, S., Waletzki, B. E., Terzic, A., Yaszemski, M. J., & Lu, L. (2016). Covalent crosslinking of graphene oxide and carbon nanotube into hydrogels enhances nerve cell responses. *Journal of Materials Chemistry B, 4*(43), 6930-6941.

Lopez, J., Xin, K., Quan, A., Xinan, K., Leto, A. A., Budihardjo, J., . . . Brandacher, G. (2018). Poly-caprolactone Nanofiber Nerve Wrap Improves Nerve Regeneration and Rodent Functional Outcomes after Delayed Nerve Repair. *Plastic and Reconstructive Surgery Global Open, 6*(4 Suppl).

Lyublinskaya, O., Borisov, Y. G., Pugovkina, N., Smirnova, I., Obidina, J. V., Ivanova, J. S., . . . Aksenov, N. (2015). Reactive oxygen species are required for human mesenchymal stem cells to initiate proliferation after the quiescence exit. *Oxidative medicine and cellular longevity, 2015*.

Marrella, A., Lagazzo, A., Barberis, F., Catelani, T., Quarto, R., & Scaglione, S. (2017). Enhanced mechanical performances and bioactivity of cell laden-graphene oxide/alginate hydrogels open new scenario for articular tissue engineering applications. *Carbon, 115*, 608-616.

Mehdizadeh, M., Weng, H., Gyawali, D., Tang, L., & Yang, J. (2012). Injectable citrate-based mussel-inspired tissue bioadhesives with high wet strength for sutureless wound closure. *Biomaterials, 33*(32), 7972-7983.

Mehrali, M., Thakur, A., Pennisi, C. P., Talebian, S., Arpanaei, A., Nikkhah, M., & Dolatshahi-Pirouz, A. (2017). Nanoreinforced Hydrogels for Tissue Engineering: Biomaterials that are Compatible with Load-Bearing and Electroactive Tissues. *Advanced Materials, 29*(8), 1603612.

Meng, X., Stout, D. A., Sun, L., Beingessner, R. L., Fenniri, H., & Webster, T. J. (2013). Novel injectable biomimetic hydrogels with carbon nanofibers and self assembled rosette nanotubes for myocardial applications. *Journal of Biomedical Materials Research Part A, 101A*(4), 1095-1102. doi:doi:10.1002/jbm.a.34400

Mottaghitalab, F., Farokhi, M., Zaminy, A., Kokabi, M., Soleimani, M., Mirahmadi, F., . . . Sadeghizadeh, M. (2013). A biosynthetic nerve guide conduit based on silk/SWNT/fibronectin nanocomposite for peripheral nerve regeneration. *PLoS One, 8*(9), e74417.

Muheremu, A., Chen, L., Wang, X., Wei, Y., Gong, K., & Ao, Q. (2017). Chitosan nerve conduits seeded with autologous bone marrow mononuclear cells for 30 mm goat peroneal nerve defect. *Scientific reports, 7*, 44002.

Omidian, H., Rocca, J. G., & Park, K. (2006). Elastic, superporous hydrogel hybrids of polyacrylamide and sodium alginate. *Macromolecular bioscience, 6*(9), 703-710.

Prang, P., Müller, R., Eljaouhari, A., Heckmann, K., Kunz, W., Weber, T., . . . Weidner, N. (2006). The promotion of oriented axonal regrowth in the injured spinal cord by alginate-based

anisotropic capillary hydrogels. *Biomaterials, 27*(19), 3560-3569. doi:https://doi.org/10.1016/j.biomaterials.2006.01.053

Reakasame, S., & Boccaccini, A. R. (2017). Oxidized alginate-based hydrogels for tissue engineering applications: A review. *Biomacromolecules, 19*(1), 3-21.

Rebowe, R., Rogers, A., Yang, X., Kundu, S., Smith, T. L., & Li, Z. (2018). Nerve repair with nerve conduits: problems, solutions, and future directions. *Journal of hand and microsurgery*.

Rowley, J. A., Madlambayan, G., & Mooney, D. J. (1999). Alginate hydrogels as synthetic extracellular matrix materials. *Biomaterials, 20*(1), 45-53. doi:https://doi.org/10.1016/S0142-9612(98)00107-0

S.Sh. Homaeigohar, H. Mahdavi, & Elbahri, M. (2012). Extraordinarily water permeable sol gel formed nanocomposite nanofibrous membranes. *Journal of colloid and interface science, 366*, 51-56.

Sadi, A. Y., Shokrgozar, M., Homaeigohar, S. S., Hosseinalipour, M., Khavandi, A., & Javadpour, J. (2006). The effect of partially stabilized zirconia on the biological properties of HA/HDPE composites in vitro. *Journal of Materials Science: Materials in Medicine, 17*(5), 407-412.

Salvetat-Delmotte, J.-P., & Rubio, A. (2002). Mechanical properties of carbon nanotubes: a fiber digest for beginners. *Carbon, 40*(10), 1729-1734. doi:https://doi.org/10.1016/S0008-6223(02)00012-X

Shen, W., & Hsieh, Y.-L. (2014). Biocompatible sodium alginate fibers by aqueous processing and physical crosslinking. *Carbohydrate Polymers, 102*, 893-900.

Shi, G., Rouabhia, M., Wang, Z., Dao, L. H., & Zhang, Z. (2004). A novel electrically conductive and biodegradable composite made of polypyrrole nanoparticles and polylactide. *Biomaterials, 25*(13), 2477-2488.

Shi, Z., Gao, X., Ullah, M. W., Li, S., Wang, Q., & Yang, G. (2016). Electroconductive natural polymer-based hydrogels. *Biomaterials, 111*, 40-54. doi:https://doi.org/10.1016/j.biomaterials.2016.09.020

Shin, S. R., Shin, C., Memic, A., Shadmehr, S., Miscuglio, M., Jung, H. Y., . . . Dokmeci, M. R. (2015). Aligned Carbon Nanotube–Based Flexible Gel Substrates for Engineering Biohybrid Tissue Actuators. *Advanced Functional Materials, 25*(28), 4486-4495. doi:doi:10.1002/adfm.201501379

Siemionow, M., & Brzezicki, G. (2009). Current techniques and concepts in peripheral nerve repair. *International review of neurobiology, 87*, 141-172.

Spinks, G. M., Shin, S. R., Wallace, G. G., Whitten, P. G., Kim, S. I., & Kim, S. J. (2006). Mechanical properties of chitosan/CNT microfibers obtained with improved dispersion. *Sensors and Actuators B: Chemical, 115*(2), 678-684. doi:https://doi.org/10.1016/j.snb.2005.10.047

Tsai, C.-C., Hung, H.-H., Liu, C.-P., Chen, Y.-T., & Pan, C.-Y. (2012). Changes in plasma membrane surface potential of PC12 cells as measured by Kelvin probe force microscopy. *PLoS One, 7*(4), e33849.

Wang, W., Degrugillier, L., Tremp, M., Prautsch, K., Sottaz, L., Schaefer, D. J., . . . Kalbermatten, D. (2018). Nerve repair with fibrin nerve conduit and modified suture placement. *The Anatomical Record, 301*(10), 1690-1696.

Vivó, M., Puigdemasa, A., Casals, L., Asensio, E., Udina, E., & Navarro, X. (2008). Immediate electrical stimulation enhances regeneration and reinnervation and modulates spinal plastic changes after sciatic nerve injury and repair. *Experimental Neurology, 211*(1), 180-193. doi:https://doi.org/10.1016/j.expneurol.2008.01.020

Yao, Y., Cui, Y., Zhao, Y., Xiao, Z., Li, X., Han, S., . . . Pan, J. (2018). Efect of longitudinally oriented collagen conduit combined with nerve growth factor on nerve regeneration after dog sciatic nerve injury. *Journal of Biomedical Materials Research Part B: Applied Biomaterials, 106*(6), 2131-2139.

Yari Sadi, A., Shokrgozar, M. A., Homaeigohar, S. S., & Khavandi, A. (2008). Biological evaluation of partially stabilized zirconia added HA/HDPE composites with osteoblast and fibroblast cell lines. *Journal of Materials Science: Materials in Medicine, 19*(6), 2359-2365. doi:10.1007/s10856-007-3336-7

Yin, J., Zhang, D., Xiang, Y., Wei, P., Yang, Z., Wang, Z., & Fu, J. (2018). The influence of cross-sectional morphology on the compressive resistance of polymeric nerve conduits. *Polymer, 148*, 93-100.